JOURNAL OF AIRCRAFT
Vol. 38, No. 6, November–December 2001

Numerical Determination of Circulation for a Swept Propeller

M. Tremmel* and D. B. Taulbee†
State University of New York at Buffalo, Buffalo, New York 14260
and
J. R. Sonnenmeier‡
Pennsylvania State University Erie—Behrend College, Erie, Pennsylvania 16563

A procedure for the numerical analysis of swept and unswept propellers is presented. Two FORTRAN codes have been written to calculate spanwise distributed quantities (such as circulation) as well as overall performance coefficients (such as propeller efficiency). The spacing of the propeller blades may be symmetrical or asymmetrical. The fluid is assumed to be incompressible, inviscid, and irrotational. However, certain viscosity and compressibility effects are included to enhance accuracy. The propeller blades are represented by bound vortex lines and the wake by trailing vortex lines. In accordance with these assumptions, Biot–Savart's law is used to determine the induced velocities by integration from the wake vortex sheet. In the modeling of the wake, wake contraction is neglected. The trailing vortex lines are allowed to align themselves in the direction of total (freestream plus induced) velocity at the blades. However, after the shedding, their direction is assumed to stay constant. The codes are run for a straight propeller for which experimental data exist in the literature, and results are compared. Furthermore a case for a swept propeller and a propeller with asymmetrically spaced blades are investigated.

Nomenclature

a	=	speed of sound
C_T, C_P	=	thrust/power coefficient
c	=	chord length
c_l, c_d	=	lift/drag coefficient
D	=	propeller diameter
$\mathrm{d}D/\mathrm{d}l_P$	=	drag per unit span
$\mathrm{d}\boldsymbol{L}/\mathrm{d}l_P$, $\mathrm{d}L/\mathrm{d}l_P$	=	lift per unit span
$\mathrm{d}\boldsymbol{l}_P$, $\mathrm{d}\boldsymbol{l}_T$	=	vector element of blade/trailing vortex line
$\mathrm{d}Q/\mathrm{d}r$, $\mathrm{d}T/\mathrm{d}r$	=	moment/thrust per unit radius
$\mathrm{d}\boldsymbol{w}_P$, $\mathrm{d}\boldsymbol{w}_T$	=	velocity induced by $\mathrm{d}\boldsymbol{l}_P$ and $\mathrm{d}\boldsymbol{l}_T$
$\mathrm{d}\varphi_T$	=	angular sector for vector element of trailing filament
$\boldsymbol{e}$	=	unit vector
J	=	advance ratio
l_P, l_T	=	blade/filament length coordinate
M	=	Mach number
Q	=	moment
n	=	rotational frequency
P	=	power
p	=	pitch
Re	=	Reynolds number
r, φ, z	=	cylindrical coordinates
$\boldsymbol{s}_P$, $\boldsymbol{s}_T$	=	distance vectors
T	=	thrust
V	=	advance speed
$\boldsymbol{V}_{\mathrm{ef}}$	=	effective velocity
$V_{\mathrm{ef}_{\eta,z}}$	=	magnitude of $\boldsymbol{V}_{\mathrm{ef}_{\eta,z}}$
$\boldsymbol{V}_{\mathrm{ef}_{\eta,z}}$	=	effective velocity in η–z plane
$\boldsymbol{V}_{\mathrm{ef}_{\varphi,z}}$	=	effective velocity in φ–z plane
$\boldsymbol{V}_R$	=	freestream velocity
$\boldsymbol{w}$	=	induced velocity
x, y, z	=	Cartesian coordinates
α_{ef}	=	effective angle of attack
α_i	=	induced trailing angle
β	=	pitch angle
Γ	=	circulation
δ	=	sweep angle
η	=	propeller efficiency
Θ	=	freestream velocity angle
ν	=	kinematic viscosity
ξ, η, z	=	blade span coordinates
ϱ	=	density
Ω	=	angular frequency

Received 15 November 2000; revision received 17 May 2001; accepted for publication 19 May 2001.

*Research Student, Department of Mechanical and Aerospace Engineering, 318 Jarvis Hall.
†Professor, Department of Mechanical and Aerospace Engineering, 315 Jarvis Hall.
‡Assistant Professor, Department of Mechanical Engineering, Benson 87, Station Road, Erie, PA 16563.

Introduction

BECAUSE of rising fuel costs, commercial airlines and aircraft manufacturers alike are forced to find ways to reduce the fuel consumption of their aircraft. Whereas one way to achieve this is the improvement of the aerodynamic design of the plane, another approach is to concentrate on the propulsion system. In this context, propeller propulsion becomes an interesting alternative to the jet engine because of its high efficiency and comparatively low fuel consumption. Various analytical and numerical approaches have been used to date to predict the performance of propellers. One of the earliest analytical theories is the classical momentum theory, described by, among others, Glauert[1] and McCormick,[2] where the propeller is modeled as an infinitely thin actuator disk across which the static pressure increases discontinuously. However, due to the assumptions made (such as an infinite number of blades and a constant velocity over the disk radius), momentum theory gives only a rough estimate of propeller performance and no information about the spanwise distribution of quantities such as blade loading.

Of far greater accuracy is vortex theory, which has found a host of applications in the treatment of propellers. Akin to classical lifting line theory (see Prandtl[3]), the blades are replaced by a system of bound vortex lines and trailing free vortex filaments whose strength is given by the change of bound vorticity according to the Kelvin–Helmholtz theorem. In most of these approaches, a single bound vortex line placed at the quarter-chord point of the blade is used to represent the blade. The geometry of the wake can either be prescribed [prescribed wake analysis, (PWA)], or the trailing vortex

filaments can be allowed to align themselves with the resulting flow [free wake analysis, (FWA)].

For PWA theories, the case treated most extensively has been the optimum propeller, for which the energy lost per unit time to create the trailing vortex system is a minimum and for which the wake shape is an undistorted helix (as shown by Betz and Prandtl[4]). Solutions for this case have been presented by, among others, Goldstein,[5] Theodorsen,[6] Larrabee,[7] and Drela and Larrabee.[8] In most cases of PWA theory, the induced velocities are not computed directly by integrating the effects of the trailing vortices, but instead analytical formulas are used. This was done, for example, in an approach by Adkins and Liebeck.[9] A PWA method that actually integrates the induced effects from all trailing vortex filaments was published by Ribner and Foster.[10]

In the FWA approach, by contrast, the trailing vortices are allowed to align themselves in the direction of total velocity at every point in space. This approach is very accurate, but computationally expensive. An FWA method is presented by Favier et al.,[11] where, to save computer time, the wake is divided into a near and a far region. The near region consists of the usual vortex filaments, whereas the far region, which is taken to begin where the wake has fully contracted, is modeled as semi-infinite vortex cylinders. The same idea of dividing the wake in a near and a far region was also used by Robison et al.[12]

Interestingly, most approaches to date deal with straight propellers having symmetrically spaced blades. In recent times, however, there has been an increasing interest in swept propellers due to benefits of blade sweep like the reduction of propeller noise. Because of noise considerations, it is also desirable to investigate propellers with asymmetrically spaced blades. This task has been undertaken here. Two FORTRAN codes have been developed for the detailed analysis of propellers that may be swept and that may have asymmetrically spaced blades. Overall propeller performance as well as spanwise distributions of engineering quantities have been calculated. The induced velocities are integrated directly from the trailing vortex sheet and the bound blade vortex lines. The wake shape is not prescribed a priori. Instead, the wake is allowed to follow the direction of total velocity at the blade. However, to keep computing time reasonable, wake contraction as well as change in trailing direction after the shedding are neglected.

Geometry and Governing Equations

In the following, symmetrically spaced blades are assumed. Figure 1 shows a top view of the propeller looking in the downstream direction, Fig. 2 shows velocities in the φ–z plane, and Fig. 3 shows a cut perpendicular to the quarter-chord line (η–z plane). It was assumed that the airfoil shape is constant over the span, whereas c and β may vary with r. The shape, c, and β are defined in the η–z plane. The flow is steady in the rotating coordinate system. The blades are represented by swept bound vortex lines with a vorticity distribution

$$\Gamma = \Gamma(l_P) = \Gamma(r) \tag{1}$$

With reference to Fig. 2, at each blade station a vortex filament with strength

$$\mathrm{d}\Gamma = -\left(\frac{\mathrm{d}\Gamma}{\mathrm{d}l_P}\right)\mathrm{d}l_P \tag{2}$$

is trailing downstream from $l_T = 0$ to $l_T \to \infty$. At a blade station, the angle beween $\boldsymbol{V}_R$ and the plane of rotation is

$$\Theta = \arctan(V/\Omega r) \tag{3}$$

The induced velocity is

$$\boldsymbol{w} = w_r\boldsymbol{e}_r + w_\varphi\boldsymbol{e}_\varphi + w_z\boldsymbol{e}_z \tag{4}$$

which gives a total (effective) velocity

$$\boldsymbol{V}_{\mathrm{ef}} = V_{\mathrm{ef}_r}\boldsymbol{e}_r + V_{\mathrm{ef}_\varphi}\boldsymbol{e}_\varphi + V_{\mathrm{ef}_z}\boldsymbol{e}_z \tag{5}$$

$$\boldsymbol{V}_{\mathrm{ef}} = w_r\boldsymbol{e}_r + (\Omega r + w_\varphi)\boldsymbol{e}_\varphi + (-V + w_z)\boldsymbol{e}_z \tag{6}$$

From this, the induced trailing angle is

$$\alpha_i = \arctan\left(-V_{\mathrm{ef}_z} \big/ V_{\mathrm{ef}_\varphi}\right) - \Theta \tag{7}$$

The vortex filament trailing from this station is assumed to follow the direction of $\boldsymbol{V}_{\mathrm{ef}\,\varphi,z} = V_{\mathrm{ef}_\varphi}\boldsymbol{e}_\varphi + V_{\mathrm{ef}_z}\boldsymbol{e}_z$, neglecting w_r and, thus,

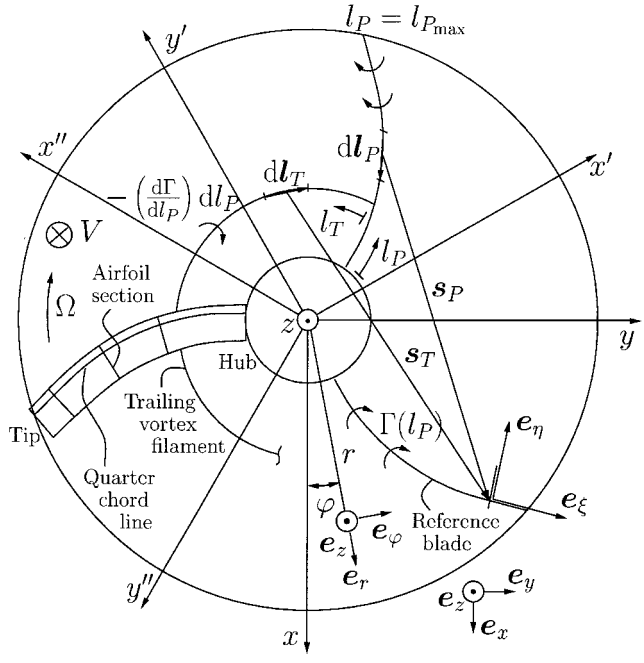

Fig. 1 Propeller geometry.

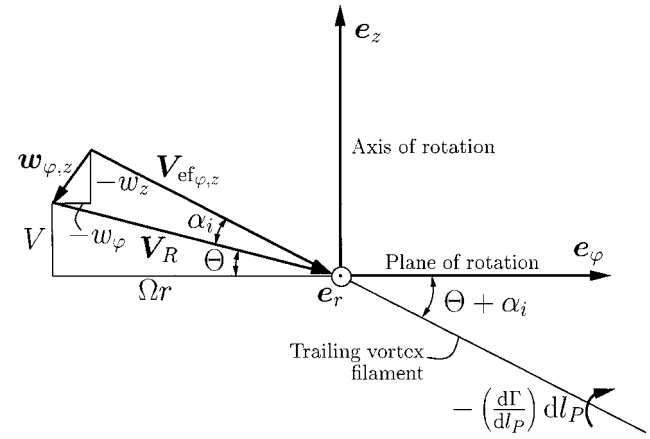

Fig. 2 Velocities in φ–z plane.

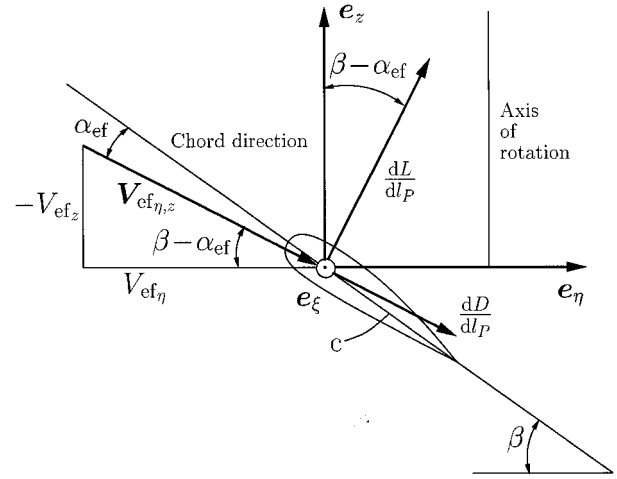

Fig. 3 Total velocity and forces at airfoil section (η–z plane).

wake contraction. Furthermore it is assumed that the trailing angle $(\Theta + \alpha_i)$ does not change once the filament has been shed.

Velocities induced by vortex lines can be determined using Biot–Savart's law (see Ref. 13). The induced velocity at a blade point is given by induced effects of trailing vortex lines and induced effects of bound vortex lines as

$$\boldsymbol{w} = \sum_B \int_{l_P=0}^{l_{P\max}} \int_{l_T=0}^{\infty} \mathrm{d}\boldsymbol{w}_T + \sum_B \int_{l_P=0}^{l_{P\max}} \mathrm{d}\boldsymbol{w}_P \tag{8}$$

Using Biot–Savart's law, we get

$$\boldsymbol{w} = \sum_B \int_{l_P=0}^{l_{P\max}} \int_{l_T=0}^{\infty} \frac{-(\mathrm{d}\Gamma/\mathrm{d}l_P)\,\mathrm{d}l_P}{4\pi} \frac{\mathrm{d}\boldsymbol{l}_T \times \boldsymbol{s}_T}{|\boldsymbol{s}_T|^3}$$

$$+ \sum_B \int_{l_P=0}^{l_{P\max}} \frac{\Gamma}{4\pi} \frac{\mathrm{d}\boldsymbol{l}_P \times \boldsymbol{s}_P}{|\boldsymbol{s}_P|^3} \tag{9}$$

where distance vectors have been introduced according to Fig. 1 and $\sum_B$ represents a summation over all blades. Equation (9) states that, when the propeller geometry, the distribution of Γ, and the distribution of α_i on the propeller blades are known, the induced velocity vector $\boldsymbol{w}$ distribution on the blade can be computed. Because α_i itself is a function of $\boldsymbol{w}$, Eq. (9) is a relationship between Γ and $\boldsymbol{w}$ on the blade.

A second relationship between Γ and $\boldsymbol{w}$ is obtained using the Kutta–Joukowski theorem. With reference to Fig. 3, the angle of attack of effective velocity in the η–z plane is

$$\alpha_{\mathrm{ef}} = \beta - \arctan\left(-V_{\mathrm{ef}_z} \big/ V_{\mathrm{ef}_\eta}\right) \tag{10}$$

where

$$V_{\mathrm{ef}_\eta} = -\sin\delta V_{\mathrm{ef}_r} + \cos\delta V_{\mathrm{ef}_\varphi} \tag{11}$$

The effective velocity magnitude in this plane is

$$V_{\mathrm{ef}_{\eta,z}} = \sqrt{V_{\mathrm{ef}_\eta}^2 + V_{\mathrm{ef}_z}^2} \tag{12}$$

from which results

$$Re = V_{\mathrm{ef}_{\eta,z}} c \big/ \nu, \qquad M = V_{\mathrm{ef}_{\eta,z}} \big/ a \tag{13}$$

The lift coefficient is

$$c_l = c_l(\mathrm{shape}, \alpha_{\mathrm{ef}}, Re, M) = \frac{\mathrm{d}L/\mathrm{d}l_P}{\frac{1}{2}\varrho V_{\mathrm{ef}_{\eta,z}}^2 c} \tag{14}$$

where "shape" denotes the airfoil geometry (for example, NACA 0010) and c_l is given for a given blade airfoil. Therefore,

$$\frac{\mathrm{d}L}{\mathrm{d}l_P} = \frac{1}{2}\varrho V_{\mathrm{ef}_{\eta,z}}^2 c_l c \tag{15}$$

With reference to Fig. 4, the Kutta–Joukowski theorem (see McCormick[14]) states

$$\mathrm{d}\boldsymbol{L} = \varrho \Gamma \boldsymbol{V}_{\mathrm{ef}} \times \mathrm{d}\boldsymbol{l}_P \tag{16}$$

$$\mathrm{d}\boldsymbol{L} = \varrho \Gamma\, \mathrm{d}l_P \left(-V_{\mathrm{ef}_z} \boldsymbol{e}_\eta + V_{\mathrm{ef}_\eta} \boldsymbol{e}_z\right) \tag{17}$$

Thus,

$$\frac{\mathrm{d}\boldsymbol{L}}{\mathrm{d}l_P} = \varrho \Gamma \left(-V_{\mathrm{ef}_z} \boldsymbol{e}_\eta + V_{\mathrm{ef}_\eta} \boldsymbol{e}_z\right) \tag{18}$$

$$\frac{\mathrm{d}L}{\mathrm{d}l_P} = \varrho \Gamma V_{\mathrm{ef}_{\eta,z}} \tag{19}$$

Combining Eq. (19) with Eq. (15), we get

$$\Gamma = \tfrac{1}{2} V_{\mathrm{ef}_{\eta,z}} c_l c \tag{20}$$

which is a second relation between $\boldsymbol{w}$ and Γ at a blade station.

When Eq. (20) is written as $\boldsymbol{w} = f(\Gamma)$ and inserted in Eq. (9), a single integrodifferential equation is obtained for Γ:

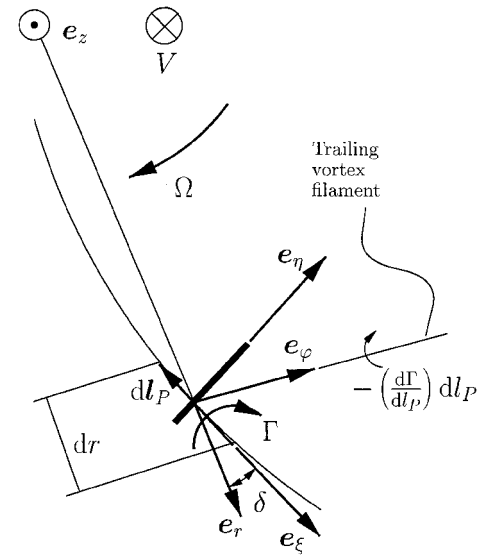

Fig. 4 Geometry for Kutta–Joukowski law.

$$f(\Gamma) = \sum_B \int_{l_P=0}^{l_{P\max}} \int_{l_T=0}^{\infty} \frac{-(\mathrm{d}\Gamma/\mathrm{d}l_P)\,\mathrm{d}l_P}{4\pi} \frac{\mathrm{d}\boldsymbol{l}_T \times \boldsymbol{s}_T}{|\boldsymbol{s}_T|^3}$$

$$+ \sum_B \int_{l_P=0}^{l_{P\max}} \frac{\Gamma}{4\pi} \frac{\mathrm{d}\boldsymbol{l}_P \times \boldsymbol{s}_P}{|\boldsymbol{s}_P|^3} \tag{21}$$

This equation requires two boundary conditions (at the blade tip and hub) and is equivalent to the fundamental equation of Prandtl's lifting line theory (see Anderson[15]). As boundary conditions, zero hub and tip circulation were stipulated.

In the case of asymmetrically spaced blades, the preceding equations are still valid, the only difference being that the bound circulation distribution varies from blade to blade.

Solution Algorithm and Discretization

The blades were discretized as Jm vector elements $\mathrm{d}\boldsymbol{l}_P$, and the vortex filaments as Im vector elements $\mathrm{d}\boldsymbol{l}_T$, each occupying an angular sector $\mathrm{d}\varphi_T$. Thus, the number of downstream turns considered for the filaments was limited to $TRNS = (Im \times \mathrm{d}\varphi_T)/360$ deg. A filament was taken to trail between two adjacent $\mathrm{d}\boldsymbol{l}_P$, such that $Km = Jm - 1$ filaments trail from each blade. It is assumed that the circulation value associated with a vortex line vector ($\mathrm{d}\boldsymbol{l}_P$ or $\mathrm{d}\boldsymbol{l}_T$) is the value at its midpoint. For the integration of $\mathrm{d}\boldsymbol{l}_P$ in Eq. (21), this corresponds to a trapezoidal integration rule that is of second order. The integration of $\mathrm{d}\boldsymbol{l}_T$ in Eq. (21) produces no such error because the circulation of a trailing vortex line is constant.

Starting with an initial guess for α_i and Γ on the blades, the distribution of $\boldsymbol{w}$ was obtained from Eq. (9), where the integrals were replaced by sums from 1 to Jm, Km, and Im, respectively. From $\boldsymbol{w}$, the corresponding distributions of $\boldsymbol{V}_{\mathrm{ef}}$, α_i, $V_{\mathrm{ef}_{\eta,z}}$, α_{ef}, Re, M, and c_l were calculated. Subsequently, a new value for Γ was obtained using Eq. (20), and the boundary conditions were enforced. When Γ was updated using underrelaxation, this was repeated until Γ had converged. Then α_i was updated using underrelaxation, and the procedure was redone from the start until α_i had converged as well. A computer code in FORTRAN that implements the preceding procedure has been written by Tremmel.[16]

The numerical scheme was very stable, and convergence could always be achieved, even for bad initial guesses of the distributions α_i and Γ. An initial distribution $\alpha_i = 0$ and an initially elliptic distribution of Γ yielded a low number of iterations and was the preferred choice. The inner iteration loop on Γ required strong underrelaxation, with a relaxation factor in the range from 0.1 to 0.2, whereas for the outer loop on α_i, a relaxation factor in the range from 0.8 to 0.9 has been appropriate.

To substantiate the accuracy of the solution, two grid refinement studies have been performed. First, the dependence of the solution

on the grid spacing ($d\varphi_T$) was investigated. It was found that for values of $d\varphi_T$ less than 1.0 deg the solution changes were less than 1%. Second, the dependence of the solution on the number of downstream turns (*TRNS*) of the trailing vortices was investigated. It was found that for values of *TRNS* greater than 1.0, changes in the solution did not exceed 1%. Therefore $d\varphi_T = 1$ deg and $TRNS = 1.0$ have been used in the subsequent results.

Performance Coefficients

The overall propeller performance can be described using several dimensionless coefficients. Starting from the converged distributions of $V_{\mathrm{ef}_{\eta,z}}$, c_l, Re, and M, the lift and drag force per unit span are (refer to Fig. 3)

$$\frac{dL}{dl_P} = \frac{1}{2}\varrho V_{\mathrm{ef}_{\eta,z}}^2 c_l c \tag{22}$$

$$\frac{dD}{dl_P} = \frac{1}{2}\varrho V_{\mathrm{ef}_{\eta,z}}^2 c_d c \tag{23}$$

where c_d is obtained from

$$c_d = c_d(\text{shape},\ c_l,\ Re,\ M) \tag{24}$$

for the given blade airfoil. Then, the thrust and moment per unit radius is

$$\frac{dT}{dr} = \left[\frac{dL}{dl_P}\cos(\beta - \alpha_{\mathrm{ef}}) - \frac{dD}{dl_P}\sin(\beta - \alpha_{\mathrm{ef}})\right]\frac{1}{\cos\delta} \tag{25}$$

$$\frac{dQ}{dr} = \left[\frac{dL}{dl_P}\sin(\beta - \alpha_{\mathrm{ef}}) + \frac{dD}{dl_P}\cos(\beta - \alpha_{\mathrm{ef}})\right]r \tag{26}$$

and the total thrust and moment is

$$T = Bm\int_{r=r_{\mathrm{hub}}}^{r_{\mathrm{tip}}} \frac{dT}{dr}\,dr \tag{27}$$

$$Q = Bm\int_{r=r_{\mathrm{hub}}}^{r_{\mathrm{tip}}} \frac{dQ}{dr}\,dr \tag{28}$$

where Bm equals the number of blades. The shaft power is $P = Q\Omega$, and the torque and power coefficients are

$$C_T = T/\varrho n^2 D^4 \tag{29}$$

$$C_P = P/\varrho n^3 D^5 \tag{30}$$

When the advance ratio is defined as

$$J = V/nD \tag{31}$$

the propeller efficiency is computed by

$$\eta = C_T\, J/C_P \tag{32}$$

Results

Straight Blades

To test the approach taken in the present work, a straight propeller for which experimental data existed (Sundar[17] and Witkowski et al.[18]) was investigated numerically. The propeller was a two-bladed model built at Purdue University (see Ref. 17) with $r_{\mathrm{tip}} = 0.0254$ m, $r_{\mathrm{hub}} = 0.1524$ m, and a constant chord length $c = 0.0508$ m. The twist distribution was given by

$$\beta(r/r_{\mathrm{tip}}) = 85.20\,\text{deg} - 105.08\,\text{deg}\,\tfrac{1}{2}(r/r_{\mathrm{tip}}) - 338.80\,\text{deg}\,\tfrac{1}{4}(r/r_{\mathrm{tip}})^2 + 1351.45\,\text{deg}\,\tfrac{1}{8}(r/r_{\mathrm{tip}})^3 - 1271.84\,\text{deg}\,\tfrac{1}{16}(r/r_{\mathrm{tip}})^4 + 1.1\,\text{deg} \tag{33}$$

A plot of the propeller geometry is shown in Fig. 5. The blade airfoil was a NACA 0010. The data were given for $M \approx 0.10 - 0.15$ and

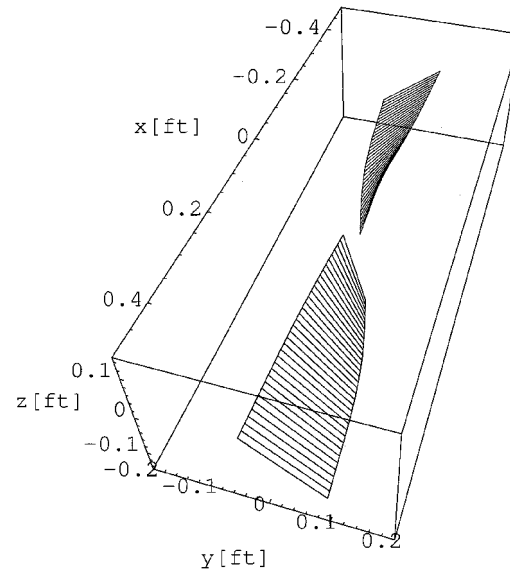

Fig. 5 Purdue propeller geometry.

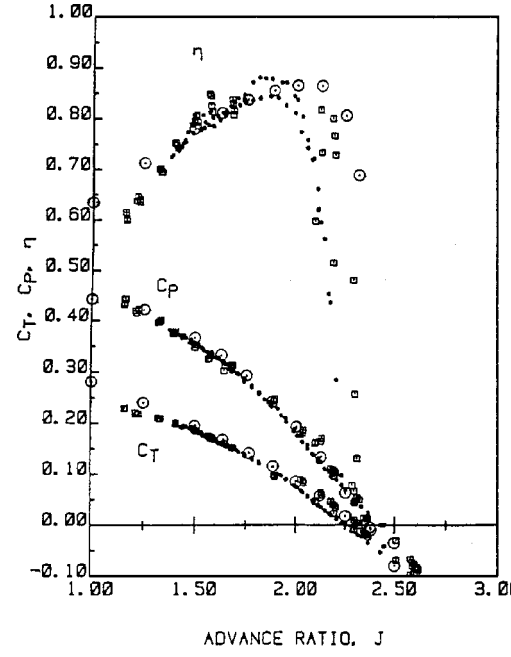

Fig. 6 Experimental (from Witkowski et al.[18]) and numerical (⊙) results for Purdue propeller.

$Re \approx 1.5 \times 10^5$–$2.0 \times 10^5$. Experimental data for c_l and c_d were obtained from Abbott and Von Doenhoff[19] at $Re = 3 \times 10^6$. Whereas the data for c_l are quite independent of Reynolds number, the values of c_d increase with decreasing Reynolds number. Therefore, c_d was slightly underestimated in the numerical analysis. Also, the value of c_l was taken to remain at the maximum in the poststall region. Figure 6 shows a comparison of experimental and numerical results. Generally, very good agreement is observed. For very low advance ratios, C_T is slightly overestimated (and C_P underestimated) because of the relative importance of viscous drag at small blade loadings. For high advance ratios, where some of the blades are stalled, C_T is again slightly overestimated (and C_P underestimated) because of the model for the lift curve. Calculated distributions of circulation, lift coefficient and induced trailing angle are shown in Figs. 7–9. Note the partial stalling of the blade for an advance ratio of $J = 1.0$ in Figs. 7–9. Figure 10 shows the spanwise distribution of induced velocities for $J = 1.5$. Note that the radial induced velocity w_r is indeed small compared to the other two components, w_φ and

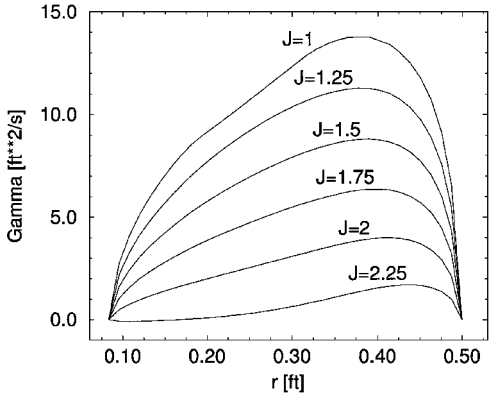

Fig. 7 Circulation distribution on Purdue propeller.

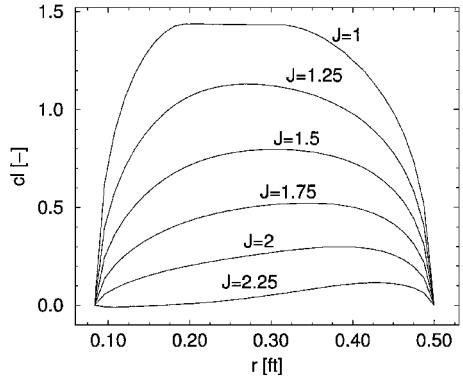

Fig. 8 Lift coefficient distribution for Purdue propeller.

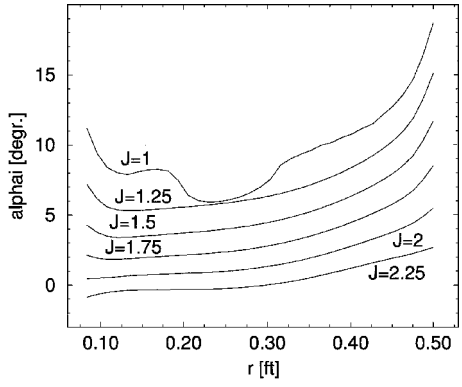

Fig. 9 Distribution of induced trailing angle for Purdue propeller.

w_z, justifying neglecting wake contraction. Finally, Fig. 11 shows the converged wake shape for $J = 1.5$. The increase in α_i close to the hub and tip of the blades is reflected in a downward curving of the wake in these regions.

Swept Blades

To investigate the effect of blade sweep, a constant pitch propeller with a pitch value of $p = 1.5$ m, $r_{\text{hub}} = 0.05$ m, and $r_{\text{tip}} = 0.8$ m was considered with and without sweep of the blades. The pitch angle was

$$\beta = \arctan(p/2\pi r \cos\delta) \tag{34}$$

This pitch angle distribution means that for $J = p/D = 0.9375$, the freestream velocity vector in the η–z plane is aligned everywhere with the chord direction. The airfoil was a NACA 4415 with $c = 0.15$ m. In the present case, $M \approx 0.05 - 0.15$ and $Re \approx 2.0 \times 10^5$–$5.0 \times 10^5$. Data for c_l and c_d were again taken from Abbott and Von Doenhoff[19] for $Re = 3 \times 10^6$. Again, the decrease

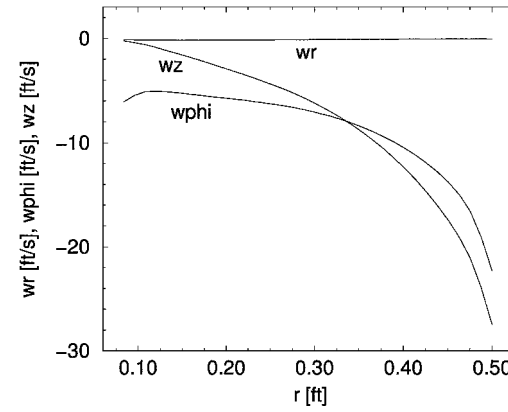

Fig. 10 Induced velocities for Purdue propeller at $J = 1.5$.

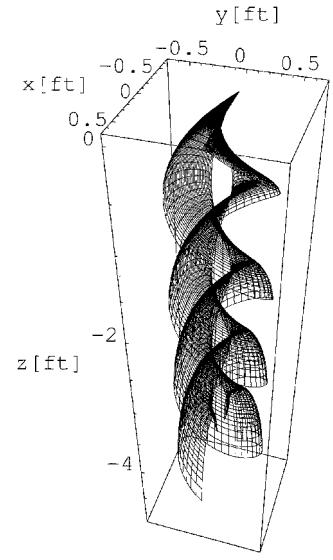

Fig. 11 Converged wake shape (both blades) for Purdue propeller at $J = 1.5$.

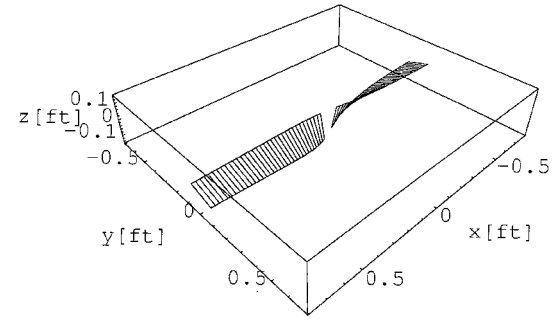

Fig. 12 Geometry of straight ($\varphi_{\text{tip}} = 0$ deg) propeller.

of c_l in the poststall region has been neglected. For the straight propeller, the quarter-chord line was a radial line, whereas for the swept propeller, its φ coordinate was increased linearly from 0 deg at the hub to 60 deg at the tip. This results in a sweep angle distribution for the swept propeller ranging from $\delta = 4.72$ to 47.52 deg. Note that the swept propeller has a larger wing surface area than the straight one because both geometries have the same hub and tip radius. Figures 12 and 13 show the geometry for the two cases, whereas Figs. 14 and 15 show the corresponding performance coefficients.

Note that the swept model has a lower C_T and C_P than the straight model, which is a result of the reduced freestream component ($\Omega r \cos\delta$) in the η–z plane of the swept propeller. Nevertheless, sweeping resulted in a higher maximum value for η, which is desirable. The spanwise distribution of c_l for both propellers is shown in Fig. 16. Note that sweep has the tendency to increase the loading at

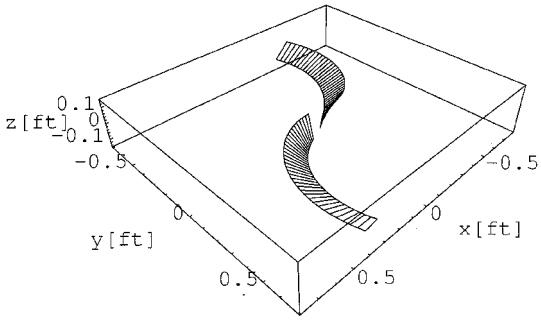

Fig. 13 Geometry of swept ($\varphi_{tip} = 60$ deg) propeller.

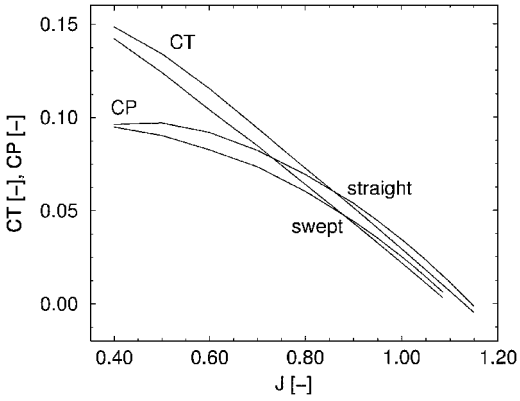

Fig. 14 Thrust and power coefficients for straight and swept propeller.

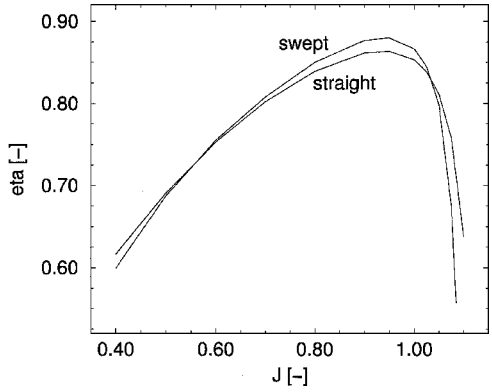

Fig. 15 Efficiency for straight and swept propeller.

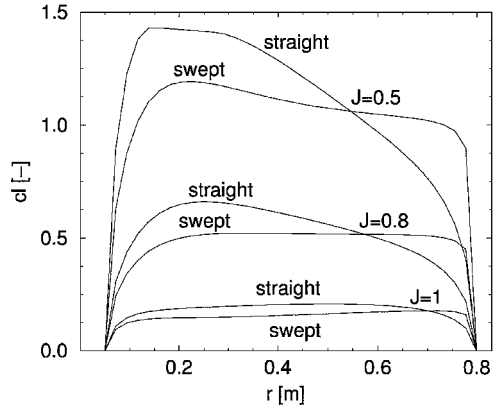

Fig. 16 Lift coefficient distribution for straight and swept propeller.

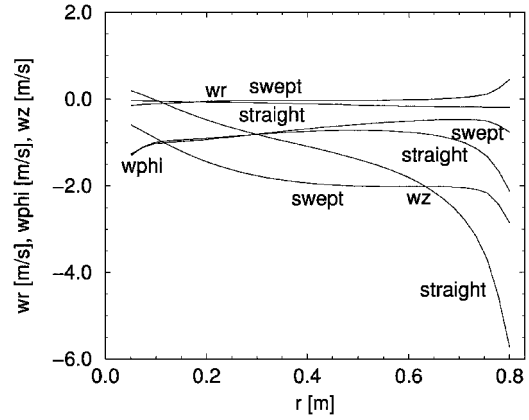

Fig. 17 Induced velocities for straight and swept propeller at $J = 0.7$.

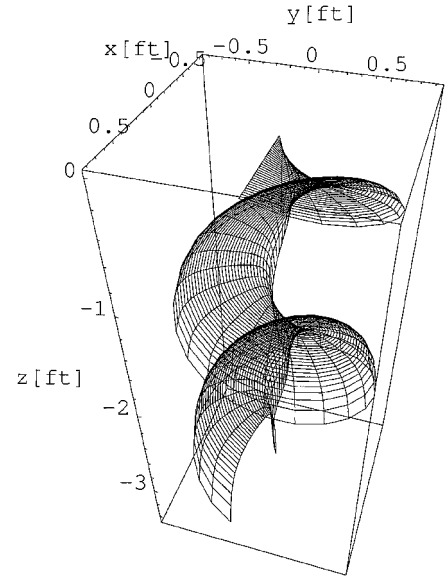

Fig. 18 Converged wake for straight propeller at $J = 0.7$.

the wing tips, producing a more even c_l distribution. Consequently, at $J = 0.5$ in Fig. 16, the straight propeller blade is partly stalled, whereas the swept blade is still free of stall. Because, in reality, c_l decreases in the poststall region, a higher maximum thrust could be achieved with the swept propeller by operating it just below stalling everywhere on the blade. Figure 17 shows the induced velocity distribution for an advance ratio of 0.7. For the swept propeller, the magnitude of w_r at the blade tip is comparable to w_φ. Thus, neglecting wake contraction might lead to inaccuracies in the swept case. Finally, Figs. 18 and 19 show the converged wake shapes for the straight and swept propeller (with only one blade shown for clarity at $J = 0.7$). The swept propeller exhibits a less distorted wake shape, which is consistent with the more even distribution of the lift coefficient.

Asymmetrically Spaced Blades

To explore the effect of asymmetrical blade spacing, two straight constant pitch propellers ($p = 1.5$ m) with $r_{hub} = 0.05$ m and $r_{tip} = 0.6$ m have been considered, each having four blades. For the symmetrical case, the blades were put at 90-deg angles, whereas for the asymmetrical case, the angles between the blades were 30 and 180 deg, respectively. The geometry is shown in Figs. 20 and 21, where the blades are numbered from 1 to 4. The airfoil was a NACA 4415 with a constant chord of $c = 0.12$ m. The same c_l and c_d data as in the earlier cases were used. The performance coefficients for both propellers are shown in Figs. 22 and 23. Asymmetry had the effect of reducing both C_T and C_P, the decrease of the former offsetting the latter, such that η decreased as well. The spanwise distributions of

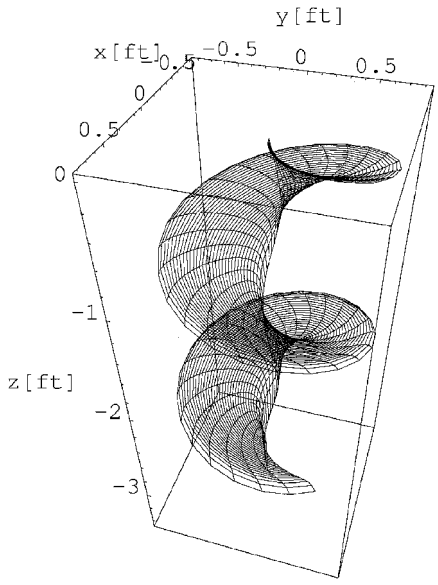

Fig. 19 Converged wake for swept propeller at $J = 0.7$.

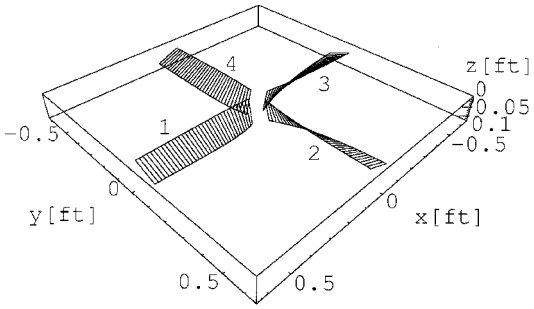

Fig. 20 Geometry of propeller with symmetrically spaced blades.

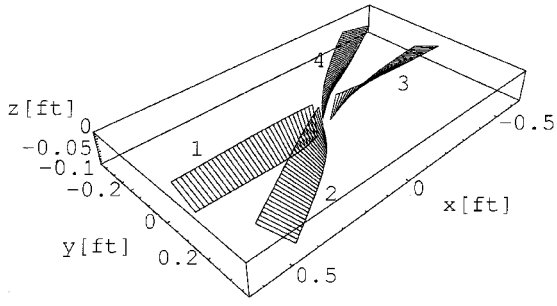

Fig. 21 Geometry of propeller with asymmetrically spaced blades.

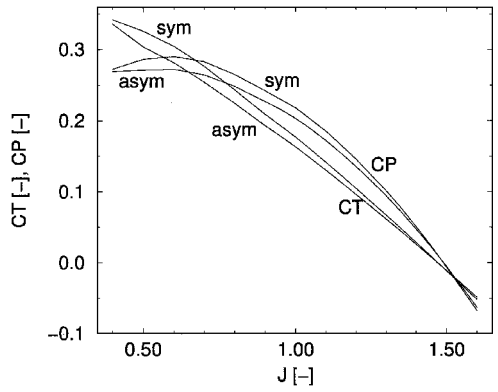

Fig. 22 Thrust and power coefficients for symmetric and asymmetric propeller.

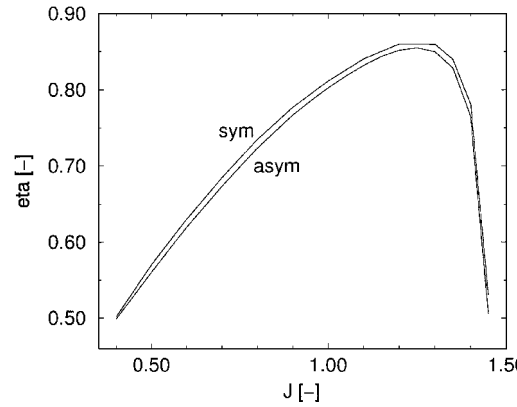

Fig. 23 Propeller efficiency for symmetric and asymmetric propeller.

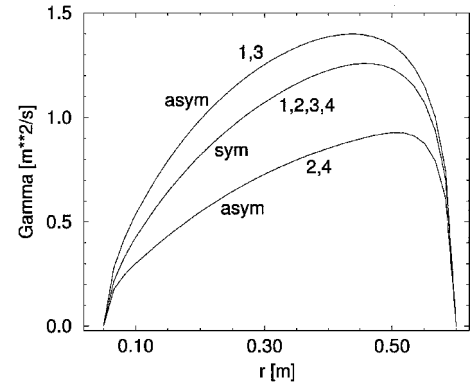

Fig. 24 Circulation distribution for symmetric and asymmetric propeller, $J = 0.9$.

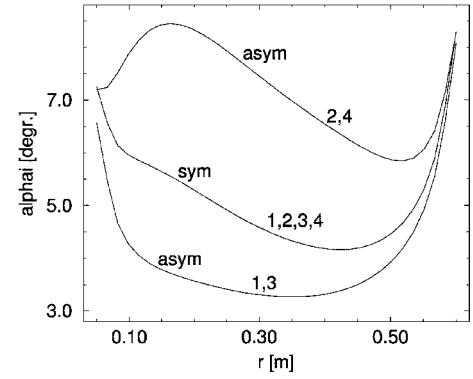

Fig. 25 Distribution of induced trailing angle for symmetric and asymmetric propeller, $J = 0.9$.

Γ and α_i for $J = 0.9$ are shown in Figs. 24 and 25. The dependence of spanwise quantities on blade number for the asymmetric case is clearly demonstrated. Values for the symmetric case lie in between values for the asymmetric case. Note that the trailing blades in the asymmetric case have higher values of α_i than the leading blades. The reason is the relative closeness of the wake being shed from the leading blades, resulting in larger induced effects on the trailing blades. A consequence of the higher values of α_i on the trailing blades is a smaller α_{ef} and, therefore, smaller values of Γ and c_l.

Conclusions

In the present work, a research tool has been developed to investigate the performance and the spanwise distributions of engineering quantities for straight or swept propellers having symmetrically or asymmetrically spaced blades. For the case of the Purdue propeller, excellent agreement has been achieved with experimental data. Furthermore, it was shown that blade sweeping results in a

slightly increased maximum efficiency and a more even spanwise distribution of the lift coefficient, preventing partial stalling even at high blade loadings. It also was demonstrated that asymmetric spacing of the blades reduces the propeller efficiency and leads to a dependence of spanwise quantities on the blade number, the trailing blades experiencing greater induced effects than the leading blades, which results in smaller values of the circulation and the lift coefficient.

References

[1]Glauert, H., *The Elements of Aerofoil and Airscrew Theory*, Macmillan, New York, 1943, pp. 199–207.

[2]McCormick, B. W., *Aerodynamics of V/STOL Flight*, Academic Press, New York, 1967, pp. 73–79.

[3]Prandtl, L., "Applications of Modern Hydrodynamics to Aeronautics," NACA TR 116, 1921, pp. 7–61.

[4]Betz, A., and Prandtl, L., *Vier Abhandlungen zur Hydrodynamik und Aerodynamik*, Selbstverlag des Kaiser-Wilhelm-Instituts für Strömungsforschung, Göttingen, Germany, 1927, pp. 68–92.

[5]Goldstein, S., "On the Vortex Theory of Screw Propellers," *Proceedings of the Royal Society of London*, Series A, Vol. 123, London, 1929, pp. 440–465.

[6]Theodorsen, T., *Theory of Propellers*, McGraw–Hill, New York, 1948, pp. 6–22.

[7]Larrabee, E. E., "Five Years Experience with Minimum Induced Loss Propellers—Part 1: Theory," SAE Technical Paper 840026, 1984.

[8]Drela, M., and Larrabee, E., *Design and Analysis of Efficient Propellers*, MIT Press, Cambridge, MA, 1986, pp. 5–28.

[9]Adkins, C. N., and Liebeck, R. H., "Design of Optimum Propellers," AIAA Paper 83-0190, Jan. 1983.

[10]Ribner, H. S., and Foster, S. P., "Ideal Efficiency of Propellers: Theodorsen Revisited," *Journal of Aircraft*, Vol. 27, No. 9, 1990, pp. 810–819.

[11]Favier, D., Ettaouil, A., and Maresca, C., "Numerical and Experimental Investigation of Isolated Propeller Wakes in Axial Flight," *Journal of Aircraft*, Vol. 26, No. 9, 1989, pp. 837–846.

[12]Robison, D. J., Coton, F. N., Roderick, A. M., and Vezza, M., "The Development of a Prescribed Wake Model for Performance Prediction in Steady Yawed Flow," SED-Vol. 16, Wind Energy—1995, Solar Energy Division, American Society of Mechanical Engineers, 1995.

[13]Spurk, J. H., *Strömungslehre*, 3rd ed., Springer-Verlag, Berlin, 1993, pp. 114, 115.

[14]McCormick, B. W., "The Application of Vortex Theory to the Optimum Swept Propeller," AIAA Paper 84-0036, Jan. 1984.

[15]Anderson, J. D., Jr., *Fundamentals of Aerodynamics*, 2nd ed., McGraw–Hill, New York, 1991, pp. 324–329.

[16]Tremmel, M., "The Numerical Determination of Circulation for a Swept Propeller," M.S. Thesis, Dept. of Mechanical and Aerospace Engineering, State Univ. of New York at Buffalo, Buffalo, NY, Aug. 1996.

[17]Sundar, R. M., "An Experimental Investigation of Propeller Wakes Using a Laser Doppler Velocimeter," Ph.D. Dissertation, Dept. of Aeronautics and Astronautics, Purdue Univ., West Lafayette, IN, April 1985, pp. 26–51.

[18]Witkowski, D. P., Lee, A. K. H., and Sullivan, J. P., "Aerodynamic Interaction Between Propellers and Wings," *Journal of Aircraft*, Vol. 26, No. 9, 1989, pp. 829–836.

[19]Abbott, I. H., and Von Doenhoff, A. E., *Theory of Wing Sections*, McGraw–Hill, New York, 1949, pp. 452–490.